Reflectance of Multilayer Gratings in the Soft X-ray Region

Eiji ISHIGURO, Tsutomu KAWASHIMA, Koujun YAMASHITA*, Hideyo KUNIEDA*, Yuzuru TAWARA*, Takashi YAMAZAKI*, Hidenori YOSHIOKA*, Akihiro FURUSAWA*, Kuninori SATO#, Masaru KOEDA$, Tetsuya NAGANO$ and Kazuo SANO$

Department of Applied Physics, Osaka City University, Sumiyoshiku, Osaka 558
*Department of Physics, Nagoya University, Chikusaku, Nagoya 464-01
#National Institute for Fusion Science, Chikusaku, Nagoya 464-01
$Optical Devices Dept., Shimadzu Corporation, Kyoto 604

The reflectance for a laminar Pt/C multilayer grating has been measured in the region from 1.2 keV to 2.8 keV by using monochromatized light from a crystal monochromator in the BL7A beamline of UVSOR. The grating comprises 10 layers of Pt and C with 2d=100 Å on a SiO_2 laminar grating which was produced by means of a holographic exposure and reactive ion-beam etching. The groove density was 1200 l/mm and the groove depth 100 Å.

Examples of angular distributions of diffracted light for various incident angle at the photon energy of 1.2 keV are shown in Fig.1. It can be seen that the intensities of the m=0,+1, and −1 spectral orders vary depending on the incident glancing angle. In Fig.2(a), the reflectance of each order are plotted as a function of the glancing angle, together with the total reflectance measured with a detector having a large acceptance angle and that of a multilayer mirror which was fabricated at the same time when the multilayer was deposited on the grating. A high total reflectance at the glancing angle less than 2 deg. are due to the total reflection of Pt, and a peak around the glancing angle of 5.8 deg. to Bragg reflection of the multilayer.

The dependence of the reflectance of the spectral orders in the Bragg peak on the glancing angle can be qualitatively interpreted by a kinematical theory of multilayer gratings[1];

$$I=\frac{1}{N^2}\frac{\sin^2\{N\pi D/\lambda(\cos\theta-\cos\theta')\}}{\sin^2\{\pi D/\lambda(\cos\theta-\cos\theta')\}}\times\frac{1}{M^2}\frac{\sin^2\{M\pi d/\lambda(R_\theta\sin\theta-R_\theta\sin\theta')\}}{\sin^2\{\pi d/\lambda(R_\theta\sin\theta-R_\theta\sin\theta')\}}$$
$$\times\left|\frac{1}{D}\int_0^L\exp\{2\pi ix(\cos\theta-\cos\theta')/\lambda\}dx\right|^2 \qquad (1)$$

The symbols in this formula are referred to the reference (1). Fig.2(b) shows a comparison of the experimental results in the Brag region with those calculated from eq.(1).

The maximum reflectance of m=0, +1 and −1 order in the Bragg region were 6.4 %(5.8°), 1.8 %(5.7°) and 1.6 %(6.2°), respectively, at E=1.2 keV, 9.0 %(4.1°),2.1 %(4.3°) and 1.6 %(4.3°) at E=1.7 keV, 6.4 %(3.5°), 1.2 %(3.3°) and 1.3 %(3.2°) at E=2.0 keV, and 8.8 %(2.5°), 1.5 %(2.2°) and 1.4 %(2.0°) at E=2.8 keV.

Reference

1)W.K.Warburton, Nucl.Instrum. and Methods A291, 278 (1990)

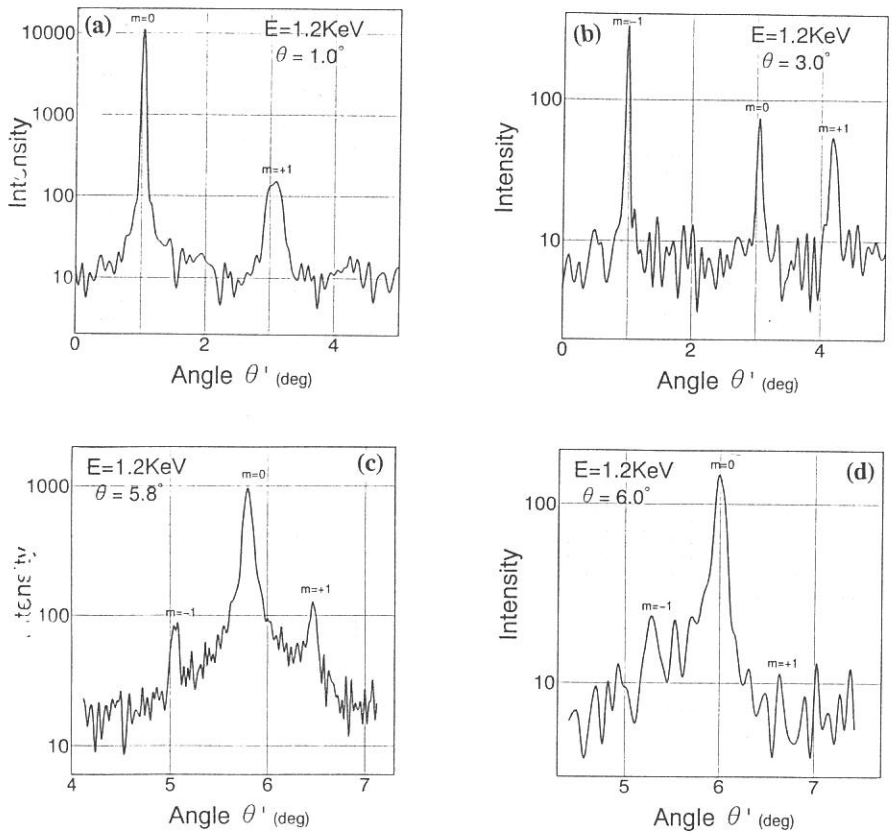

Fig.1 Angular distribution of diffracted light from a multilayer grating for various incident glancing angles θ at the photon energy of 1.2 keV.

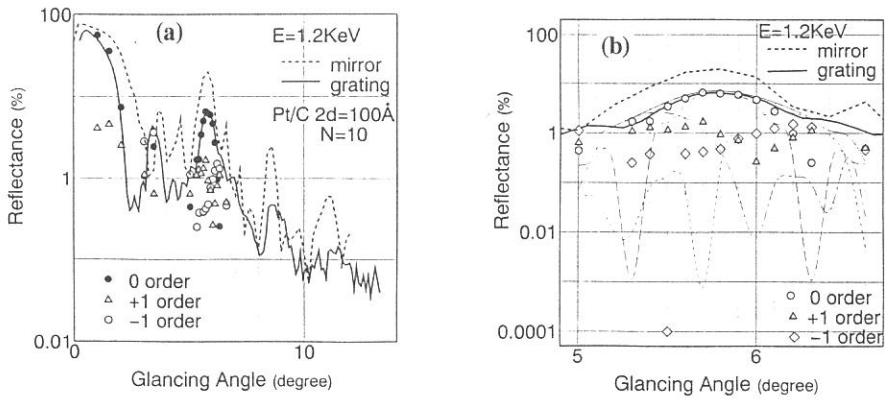

Fig.2 Reflectance of the m=0, +1 and −1 spectral orders as a function of the , incident glancing angle, together with the total reflectance of the grating(——), and that of a multilayer mirror(----). The Brag peak around the glancing angle of 5.8° is shown in an enlarged scale in fig.(b) for a comparison with theoretical results of eq.(1) for the reflectance of m=0( ), +1( ), and −1( ).

Heat Load Resistivity of SiC Gratings for High-Power Synchrotron Radiation

Eiji ISHIGURO, Makoto SAKURAI[1], Hideki MAEZAWA[2], Mihiro YANAGIHARA[3], Makoto WATANABE[4], Masaru KOEDA[5], Tetsuya NAGANO[5], Kazuo SANO[5], Yasuhiro AKUNE[6] and Kichiya TANINO[6]

Department of Applied Physics, Osaka City University, Osaka 558

[1]Department of Physics, Kobe University, Kobe 657

[2]National Laboratory for High Energy Physics, Ibaraki 305

[3]Research Institute for Scientific Measurements, Tohoku University, Sendai 980

[4]Institute for Melecular Science, Okazaki 444

[5]Shimadzu Corporation, Kyoto 604

[6]Nippon Pillar Packing Co., LTD., Hyogo 669-13

High resistivity against the heat load of synchrotron radiation is required for diffraction elements in grating monochromators which will be installed in VUV and soft x-ray beam lines of a high-brilliance next-generation storage ring. It has been reported that SiC gratings withstand high power beam emitted from an undulator.

We fabricated ion-beam etched SiC gratings and examined them about the resistivity against radiation from a multipole wiggler (EMPW #28) installed on the Photon Factory storage ring. High quality of surface finish is essential, and CVD-b SiC is considered to be one of the best mirror materials. We have developed CVD-SiC in which individual grains are strongly oriented to the (220) plane. For the fabrication methods, crystallographic orientation, polishability and etching characteristics of CVD-SiC, we described in detail elsewhere[1].

Diffraction efficiencies of two SiC gratings with groove density of 1200 l/mm were measured by using monochromatized lights in the region of 17-300 Å from a plane grating monochromator installed at the BL5B of UVSOR. One (#1) has a groove depth of 75 Å and a width-to-spacing ratio of 0.33 and the other (#2) a groove depth of 100 Å and a width-to-spacing ratio of 0.45. Through the wavelength region in the present experiment, the maximum efficiencies of the +1 order are 5-20 % for the gratings coated with Au.

The grating #1 without coating and the grating #2 coated with Au of 200 Å thickness were tested for the radiation of EMPW #28. The comparison of diffraction efficiency between Au coated and without coating revealed that the coating improves it especially just over C-K and Si-L edges. The total power which the grating absorbed was 277 W and the power density at the center of the wiggler beam was estimated to be 2.7 W/mm^2. No visible damage was observed for the grating #1, on the other hand a discoloration was observed in a limited portion around the center of irradiation for the grating #2 (Fig. 1). SEM photographs of both gratings clearly show the difference in thermal strength (Figs. 2 and 3). No deformation of the grooves was found for the grating #1, however, the grooved pattern of the grating #2 can hardly be recognized after irradiation for 40 min.

Figure 4 shows angular distributions of the diffraction light for the both gratings. The efficiencies of the grating #2 can be regarded to be unchanged after irradiation, as well as for the grating #2. However, increase of the scattered light components was observed for the grating #2 irradiated for 40 min. This is due to the disappearance of the groove pattern in the central part and relatively large deformation of the Au layer in the portion except the center.

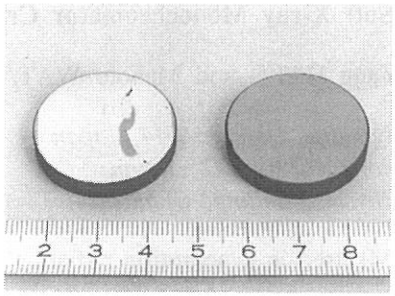

Figure 1 SiC gratings after irradiation of wiggler beams; the right side is grating #1 and the left grating #2. The left and right halves of each grating were irradiated for 4 and 40 min, respectively.

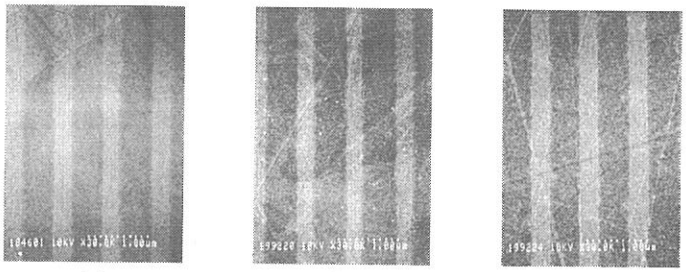

(a) (b) (c)

Figure 2 SEM photographs of the grating #1 (a) before irradiation, (b) after irradiation for 4 min and (c) after irradiation for 40 min.

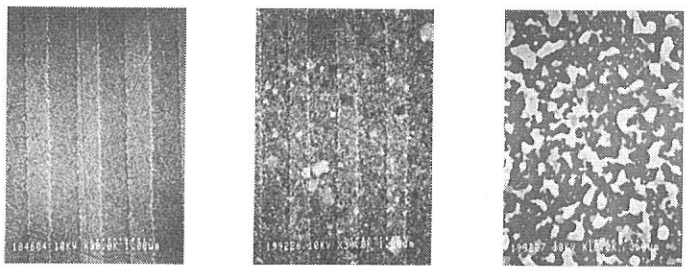

(a) (b) (c)

Figure 3 SEM photographs of the grating #2 (a) before irradiation, (b) after irradiation for 4 min and (c) after irradiation for 40 min.

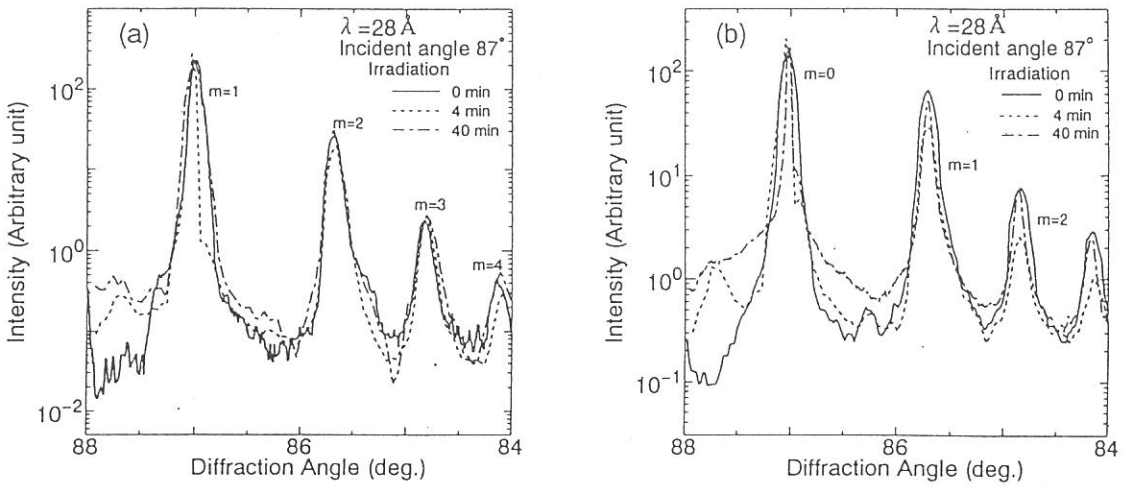

Figure 4 Angular distribution of diffraction intensities before and after irradiation for (a) the grating #1 and (b) the grating #2.

[1]E. Ishiguro, H. Maezawa et al., Proc. SPIE (to be published).

Performance Check of β-Alumina as a Soft X-ray Monochromator Crystal

Atsunari HIRAYA, Kazunori MATSUDA*, Yang HAI**, and Makoto WATANABE

Institute for Molecular Science, Myodaiji, Okazaki 444, Japan
**Naruto University of Education, Naruto 772, Japan*
***Institute of High Energy Physics, Beijing, China*

For double crystal monochromators (DXM) used in synchrotron radiation facilities, only beryl crystal can be used steadily in the region below 1.5 keV. However beryl has several disadvantages such as weakness to radiation damage and difficulty to obtain a good natural specimen. Therefore, there are interest and need for crystals that can be used below 1.5 keV, especially the lower energy region than that covered with beryl crystal. We tried to use a synthesized inorganic crystal β-alumina ($Na_2O{\cdot}(Al_2O_3)_{11}$, 2d = 22.53 Å) as a monochromator crystal of DXM and compared the resolution and intensity from β-alumina with those from beryl.

A pair of β-alumina crystals were prepared from a block of re-crystallized alumina firebrick (Toshiba Monoflux) by cleaving flat area (ca. 2 × 2 cm^2) and used without further polishing. Measurements were carried out by setting two β-alumina crystals in the DXM at BL1A beamline equipped with a focusing pre-mirror. Figure 1 shows a throughput spectra of DXM obtained with β-alumina, beryl, quartz-Y, InSb, and Ge-111 crystals with the same detection system (electron multiplier tube with Au first dynode, high voltage = 1.5 kV). The β-alumina crystal covers the energy region from 580 to 1740 eV (Bragg angle 71.5° ~ 18.5°) with more than ten times higher intensity than beryl crystal. Resolution of the pair of β-alumina crystals used is estimated to be 0.75 eV at about 900 eV which is enough narrow for some experiments such as EXAFS, though broader than that of beryl (0.46 eV). No degradation in intensity and resolution were observed even after 1 month exposure to synchrotron radiation under normal operation conditions. Since this resolution was obtained for as-cleaved crystal, improvement in both intensity and resolution are expected after proper treatment such as polishing and annealing. As an example of measurement with using β-alumina, figure 2 shows an absorption spectrum, obtained by a transmission method, of NaF film (2000 Å) deposited on a polyester film.

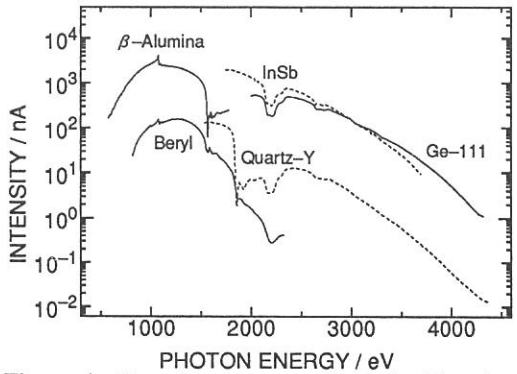

Figure 1. Throughput spectra obtained with using β-alumina, beryl, quartz-Y, InSb, Ge-111 crystals.

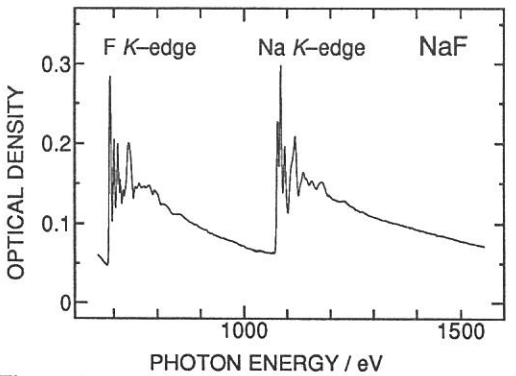

Figure 2. F-*K* and Na-*K* absorption spectrum of NaF thin film (2000Å).

X-Ray Reflectivity of Thin Foil Mirrors for X-Ray Telescope

K. Yamashita, H. Kunieda, Y. Tawara, Y. Kamata, K. Iwasawa, T. Yamazaki, A. Furusawa and H. Yoshioka

Department of Physics, Nagoya University, Nagoya 464-01

The grazing incidence X-ray telescope for ASTRO-D, the fourth Japanese X-ray astronomy satellite, is made of two stages multi-nested thin foil conical mirrors in order to reduce the weight and to get high throughput in the energy region up to 10 keV. Conical mirrors are simulated to Wolter type I. The telescope's specifications are: outer (and inner) diameter, 344 mm (and 120 mm); glancing angle of 0.25 deg at inner to 0.7 deg at outer; mirror length, 100(x2) mm; focal length, 3500 mm; total number of mirrors, 120; mirror substrate, aluminum foil (0.15 mm thick) coated with acrylic laquer and gold for the reflecting surface; angular resolution, 3 arcmin (half power diameter, HPD); and effective area of 300 cm2 at 1.5 keV, 180 cm2 at 4.5 keV and 100 cm2 at 8 keV. Aluminum foil substrates are bent in a proper shape by using a hot-press method with vacuum chucking to a conical mandrel. All the mirrors are precisely aligned at coaxial and confocal positions by 1 mm pitch in average in order to obtain sharp image at the focal plane.

The X-ray reflectivity of thin foil mirrors against glancing angles was measured by using a double crystal monochromator at BL-7A in the energy range of 0.8 - 2.3 keV with beryl and 1.7 - 4 keV with InSb. The glancing angle was changed in the range of 0.5 - 1.4 deg. A conical mirror was fixed at the sample holder

keeping in right shape. The observed results are shown in figure 1. The degradation of the reflectivity was not recognized in comparison with a standard gold mirror deposited on superpolished glass[1]. Therefore it turned out that the reflecting surface is smooth enough for X-ray reflection, whereas the surface figure is not flat enough for the image formation as expected.

This measurement is very important to derive the effective area of the telescope against X-ray energies, especially around M absorption edge of gold.

References

1. K. Yamashita et al., UVSOR Activity Report 1991, p.112.

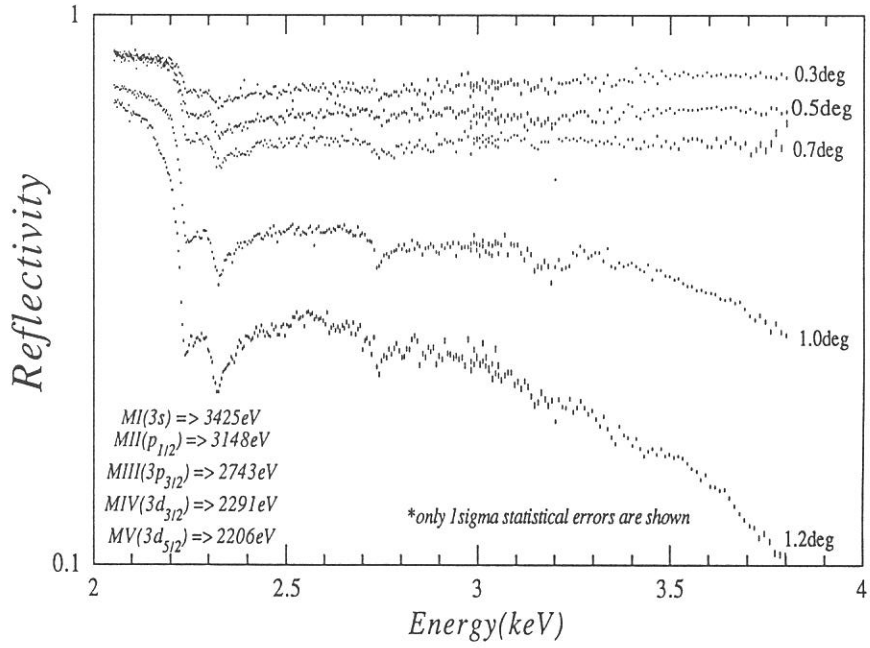

Fig.1 Reflectivity of thin foil gold mirror vs. X-ray energy. Incident angles to the reflecting surface are written in the figure.

Soft X-Ray Imaging Microscope with Sub-optical Resolution at UVSOR.

N. Watanabe[1], S. Aoki[1], Y. Shimanuki[2], K. Kawasaki[2], M. Taniguchi[3], E. Anderson[4], D. Attwood[4], D. Kern[5], S. Shimizu[6], H.Nagata[6], and H.Kihara[7]

1) Department of Applied Physics, Tsukuba University, Tsukuba
2) Department of Oral Anatomy, Tsurumi University, Yokohama
3) Department of Physics, Nagoya University, Nagoya
4) Lawrence Berkeley Laboratory, Berkeley, CA
5) IBM Research Center, Yorktown Heights, NY
6) Nikon Corp., Nishi-ooi, Shinagawa-ku, Tokyo
7) Jichi Medical School, School of Nursing, Tochigi 329-04

A soft x-ray imaging microscope with zone plates was set up at UVSOR BL8A, and imaging tests were performed at 3.2nm. This microscope is basicaly the same with the last type[1], but with great improvements on resolution, as objective zone plates of high resolution became available.

The system consists of an upstream pinhole (UPH; $100\mu m\phi$-$400\mu m\phi$ or not used), a filter (SiN, thickness: 100nm and Ti, thickness: 55nm), a condenser zone plate (($4.3mm\phi$, the outermost zone width: $0.25\mu m\phi$. The third order radiation was used for illumination.) or ($2.4mm\phi$, the outermost zone width: $0.44\mu m\phi$. The first order radiation was used for illumination.), a pinhole (SPH; $10\mu m\phi$ or $30\mu m\phi$), a specimen, an objective zone plate (OZP; $50\mu m\phi$, the outermost zone width: 45nm), a micro-channel plate (MCP) and a fluorescent plate. The magnification ratio is 750-800. A photographic view of the microscope is shown in Fig.1

The resolution was estimated to be $0.21\mu m$ from the edge profile of an image of a zone plate used as a specimen (10%-90% of the total contrast). This is worse than the theoretical one (55nm), which would be mainly due to low spatial resolution of MCP. A 78nm line and 78nm space pattern of a Ni zone plate (thickness: 135nm) was resolved as shown in Fig.2. Experiments using photographic films instead of MCP are currently under way.

Dry biological specimens, such as diatoms (of which image is shown in Fig.3), rabbit and crab myofibrils (of which image is shown in Fig.4), collagen fibers, chromosomes, sperms, Synechocystis, Porphyridium cruentum, Chlamydomonas, Euglena gracilis, and soybean protoplasts, were observed.

Acknowledgements

The authors are grateful to the help and encouragements by Prof. M. Watanabe, Mr. T. Kinoshita and other staffs of the Institute for Molecular Science. They also express their sincere thanks to all sample suppliers; rabbit myofibril (Prof. S. Ishiwata of Waseda Univ.),

crab myofibril and sperms (Prof. Y. Hamaguchi of Tokyo Inst. of Technology), collagen fibers (Dr. K. Furuya of Inst. of Physiol. Sci.), chromosomes (Dr. Y. Kinjo of Tokyo Metropolitan Inst. for Isotope Research), Synechosystis PCC6714, Porphyridium cruentum, Chlamydomonas (Dr. S. Nakamura of Inst. for Basic Biology) and Euglena gracilis (Prof. M. Watanabe of Inst. for Basic Biology).

Reference

1) N. Watanabe, Y. Shimanuki, M. Taniguchi, and H. Kihara (1992) UVSOR Activity Report, 1991, 72-73.

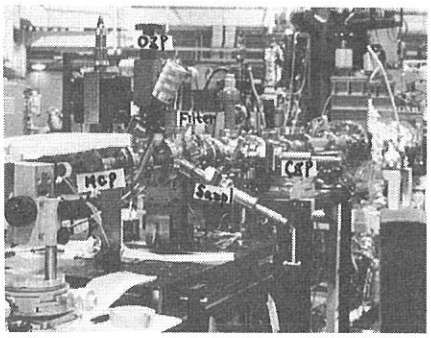

Fig.1 Photographic view of the microscope.

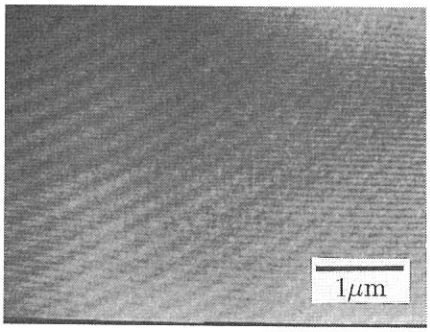

Fig.2 Image of the specimen zone plate at 3.2nm.

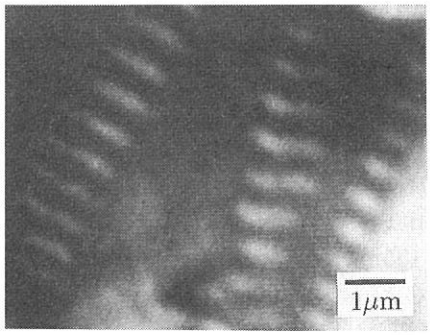

Fig.3 Image of a diatom at 3.2nm.

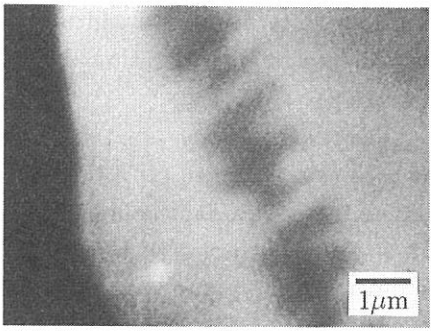

Fig.4 Image of a rabbit myofibril at 3.2nm.

Some Characteristics of a Solid State Detector at Soft X-ray Region

Hiroshi TSUNEMI, Kiyoshi HAYASHIDA, Keisuke TAMURA
Akira HIRANO and Hiroyuki MURAKAMI
Department of Earth and Space Science, Faculty of Science, Osaka University
1-1 Machikaneyama-cho, Toyonaka, Osaka, 560

We carried out a experiment to test a solid state detector, EG & G ORTEC Si(Li) detector. The entrance window of the detector is about 4 mm in diameter while we placed a pinhole of about 0.5 mm in diameter in front of the detector to restrict the position of X-rays at the detector center. We also placed an X-ray shutter to control the incident X-ray flux on the detector. All the measurements were done at an intensity level about 2000 counts/sec.

Figure 1 shows pulse height distributions for various X-ray energies. They can be well expressed with two gaussian profiles: one represents a main peak profile while the other represents a tail next to the main peak. There is a clear difference in the shape of the pulse height distribution just below the Si-K edge energy (1.84 keV) and that just above it. The ratio between the main peak and the tail part is correlated not to the incident X-ray energy but to the mean absorption length of

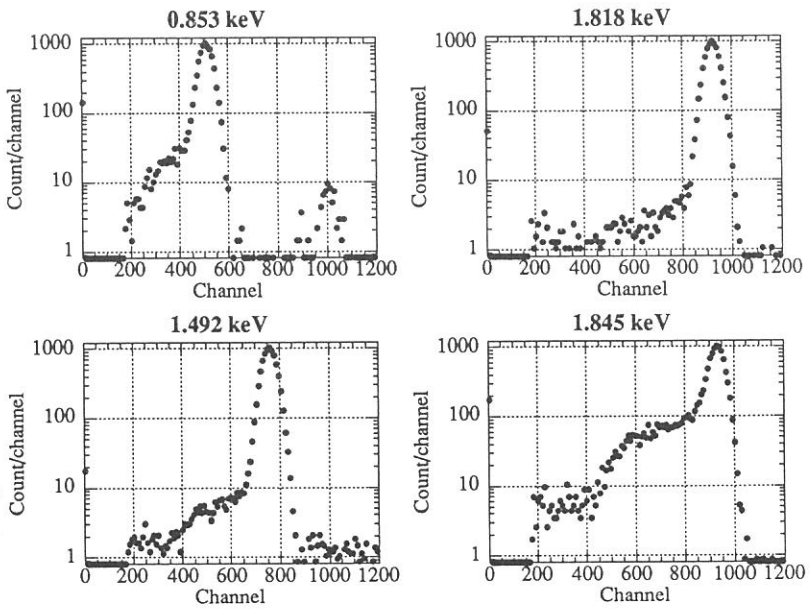

Fig. 1. Pulse height distributions obtained with the SSD at various X-ray energies. The shorter the mean absorption length is, the bigger the tail part next to the main peak. There is a big difference just above and below the Si-K edge energy.

the X-ray in silicon. The mean absorption length just above the Si-K edge is only 1.2 μm while that just above it is about 14 μm.

Taking into account the electric field applied inside the Si and the electron mobility, some charge is lost at the earth electrode due to the diffusion process. Therefore, the shorter the mean absorption length is, the bigger the tail part compared to that of the main peak. Since the mean absorption length of the X-ray below 0.7 keV becomes shorter than that at 1.84 keV, the tail part will grow until we lose the main peak. The solid state detector may not work well at sub-keV range even if we replace the beryllium window with other thin material.

Figure 2 shows the relation between the incident X-ray energy and the peak position of the main peak. In general, the linearity of the detector is good. However, there is a clear jump at the Si-K edge energy. The discrepancy is about 8 eV. The X-ray just above it is absorbed through the K-absorption while that below it is absorbed through the L-absorption. The final charge state of the atom depends on the absorption process. The average ionization degree of the atom after its K-electron vacancy is bigger than that after its L-electron vacancy. The ionization process of the photoelectron in the silicon is independent of the incident X-ray energy. This means that the average ionization energy for the X-ray just above the Si-K edge becomes bigger than that for the X-ray just below it.

We found the characteristics of Si SSD as follows.

(1) It will produce a deformed pulse height distribution when the X-ray mean absorption length is short.

(2) There is a non linearity of about 8 eV at the Si-K edge energy.

Fig. 2. The linearity of the SSD between the incident X-ray energy and the peak position of the main peak. A wide energy range is shown in the left while that around the Si-K edge is in the right. There is a non-linearity effect about 8 eV at the Si-K edge energy seen.

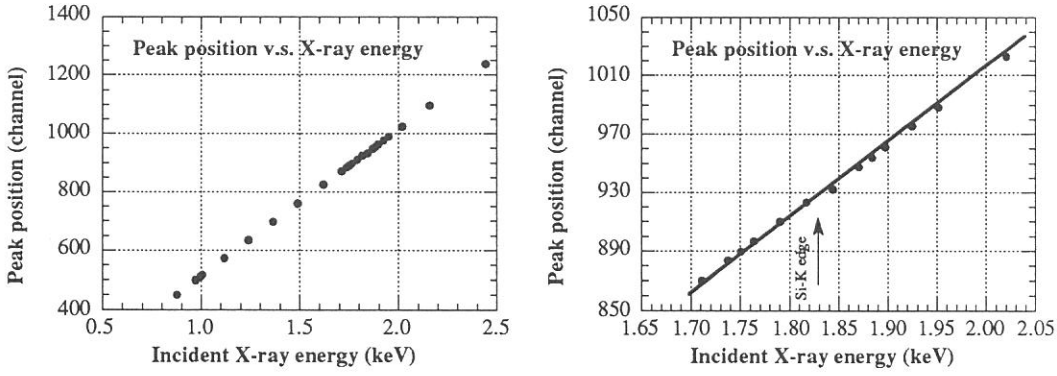

Calibration of the GIS Detectors on board the ASTRO-D Satellite

Kazuo MAKISHIMA, Yoshiki KOHMURA, Makoto TASHIRO, Yasushi IKEBE,
Takaya OHASHI*, Koujun YAMASHITA#, Yoshihiro UEDA#,
and the GIS Team

Department of Physics, University of Tokyo, Bunkyo-ku, Tokyo 113.
* Department of Physics, Tokyo Metropolitan University, Hachioji, Tokyo 192-03.
# Institute of Space and Astronautical Science, Sagamihara, Kanagawa 229.

The cosmic X-ray satellite ASTRO-D, to be launched in February 1993, will carry on board two sets of imaging gas scintillation proportional counters, called GIS (Gas Imaging Spectrometer). The GIS detectors have a circular working area of 50 mm diameter, a wide sensitivity range (0.7-15 keV), a moderate energy resolution (8% FWHM at 6 keV), and a position resolution of 0.5 mm (FWHM) because they are used as focal plane imaging X-ray detectors. The GIS detectors also have very low background level suitable for observations of very faint cosmic X-ray sources.

Because of these superior but complex capability of the GIS, it is essential to calibrate their pulse-height and position responses all over the sensitive energy range in detail before launch. The calibration needs highly monochromatic and well collimated X-ray beam of sufficient brightness. Furthermore calibration below about 4 keV is difficult to perform in the atmosphere.Therefore the UV SOR provides an ideal mean of the GIS calibration.

We used the BL7A beam line of the UV SOR to calibrate a protomodel GIS detector. Using a Ge(111) and a Beryl crystal spectrometers to cover energy ranges of 2.0-5.8 and 0.83-2.41 keV respectively, we performed detailed two-dimensional scans over the sensitive area of the detector at various beam energies. We obtained the following results. These results provide valuable contribution to the GIS project which aims at a novel research in the high energy astrophysics.

(1) We measured relation between the GIS output pulse-height and the incident beam energy (see Figure). In particular, we determined small jumps in the pulse-height vs. energy relation at L-edges of Xenon, which is used as a working gas in the GIS.

(2) We obtained deteailed calibration data of the GIS down to about 0.8 keV, which is close to its energy lower boundary.

(3) Through these calibration experiments, we confirmed that the GIS high voltage components (up tp 8 kV) work properly in the vacuum, and that the signal processing electronics (placed outside the chamber) can properly analyze the GIS analog signals down to the lower-level discriminator.

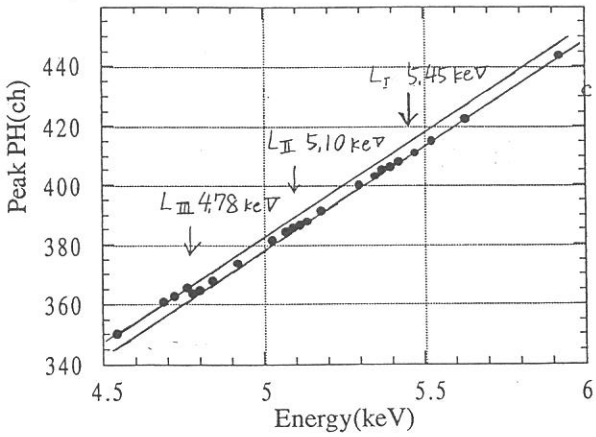

Figure: relation between the GIS output pulse height and the incident beam energy.

Finally, we deeply thank the UV-SOR staff for their kind help and cooperation